ELSEVIER

Catalysis Today 40 (1998) 273–286

CATALYSIS TODAY

Comments on the nature of the active site of vanadium phosphate catalysts for butane oxidation

Graham J. Hutchings[a,*], Christopher J. Kiely[b], Maria T. Sananes-Schulz[c], Andrew Burrows[b], Jean Claude Volta[c]

[a] *Department of Chemistry, University of Wales, Cardiff, P.O. Box 912, Cardiff CF1 3TB, UK*
[b] *Department of Materials Science and Engineering, University of Liverpool, P.O. Box 147, Liverpool, L69 3BX, UK*
[c] *Institut de Recherches sur la Catalyse, CNRS, 2 Avenue Albert Einstein, 69626, Villeurbanne Cedex, France*

Abstract

The effect of structure activity relationships for vanadium phosphorus catalysts for the oxidation of butane to maleic anhydride are described and discussed. A range of characterisation techniques including in situ laser Raman spectroscopy and transmission electron microscopy have been used on catalysts prepared by using three different methods: (i) VPA, prepared by using the standard aqueous HCl method followed by a water extraction step; (ii) VPO, prepared by the reaction of V_2O_5 with H_3PO_4 in isobutanol followed by a water extraction step; and (iii) VPD, prepared by the reaction of $VOPO_4{\cdot}2H_2O$ with isobutanol. The key results indicate that:

(a) The active site can be formed on a wide range of vanadium phosphorus containing phases due to the observation that VPA, VPO and VPD catalysts with different compositions give similar specific activity for maleic anhydride formation.
(b) The in situ LRS and TEM studies show that the hemihydrate to final catalyst transformation is complex and that after a short exposure to butane/air at temperatures >370°C the hemihydrate is transformed mainly to a disordered material. At the onset of maleic anhydride formation, there is a complex mixture of phases present, including $(VO)_2P_2O_7$ and a variety of $VOPO_4$ phases.
(c) For Co^{2+} promoted by VPO and VPD catalysts, the activity for maleic anhydride formation is a function of the concentration of the V(V) phases present.

From these studies, we conclude that the active center for butane activation and maleic anhydride formation comprise a V^{4+}/V^{5+} couple that is well dispersed on the surface of a range of VPO phases, which for well-equilibrated catalysts will be $(VO)_2P_2O_7$. This hypothesis is discussed in relation to other recent data which also indicate the importance of V^{5+} centers in the selective activation of butane to maleic anhydride. © 1998 Elsevier Science B.V.

Keywords: Vanadium phosphate catalysts; Butane oxidation; Maleic anhydride; Transmission electron microscopy; In situ laser Raman spectroscopy

1. Introduction

Vanadium phosphates represent one of the best studied heterogeneous catalyst systems. More than

*Corresponding author. Tel.: +44 1222874 805; fax: +44 1222874075.

PII S0920-5861(98)00015-7

one thousand papers and patents have addressed this subject, since it was first observed that these materials were catalysts for the oxidation of butane to maleic anhydride [1]. Early research concentrated on refining the method of preparation [2,3] or the identification of catalyst promoters [4]. It was recognised, very early on, that the most effective catalysts were prepared from precursors comprising a single compound ($VOHPO_4{\cdot}0.5H_2O$) which were transformed in situ in the reactor in the presence of butane/air to a final catalyst that comprised mainly $(VO)_2P_2O_7$ [5,6]. In recent years, considerable effort has been applied in order to gain an understanding of the nature of the active site for these catalysts. To some extent this has been aided by the use of improved in situ spectroscopic and electron microscopy techniques. Since 1992, as a result of the EC HCM project on oxidation of hydrocarbons, we have studied vanadium phosphorus catalysts using a combination of these techniques. We have concentrated our studies in two distinct areas:

(i) The control of the morphology of the initial $VOHPO_4{\cdot}0.5H_2O$ precursor.
(ii) The transformation of the precursor to the final catalysts.

These are both crucial aspects of the preparation of active catalysts and the studies were undertaken with a view to generalizing other oxide catalysts. However, the control of precursor morphology is especially important for vanadium phosphate catalysts since the precursor/final catalyst transformation is considered to be topotactic [5,7] and, hence, final catalyst morphology can be readily controlled at the precursor stage. We have found that precursor morphology can be readily modified, using a preparation route based on alcohol reduction of $VOPO_4{\cdot}2H_2O$ [8–10] which has led to the identification of a high area preparation method denoted by us as VPD [8,11,12].

The purpose of this paper is to consider in detail the work carried out on the second topic, i.e. the transformation of the precursor into the final catalyst and, in particular, to comment on the nature of the active site for selective butane activation. In this respect, the key feature of our recent papers will be reviewed and contrasted with recent noteworthy publications from other active research groups. The reason for this approach is that one of the major controversies in this field concerns whether only V^{4+} material, e.g. $(VO)_2P_2O_7$, are required as the selective catalyst or whether V^{5+} phases also play an important role [13–16].

2. Experimental

The following section sets out the preparation and characterisation details for the catalysts described in this review paper.

2.1. Catalyst preparation and testing

Three catalyst precursors are described and discussed and these are denoted by VPA, VPO and VPD. VPA was prepared by refluxing V_2O_5 (60.6 g) and aqueous HCl (35%, 790 ml) for 1.5 h, at which time the solution was dark blue in colour. H_3PO_4 (88%, 89.1 g) was added and the solution was refluxed for a further 1.5 h. The solution was then evaporated to near dryness by sidearm distillation (rate of solvent removal 100 ml h^{-1}) to a blue green paste which was dried in air (110°C, 16 h) to give a blue green solid. This solid was refluxed for 2 h with distilled water (1 g/20 ml) and then the suspension was filtered hot and dried in air (110°C, 16 h) to give a blue solid. VPO was prepared by refluxing V_2O_5 (11.8 g) with H_3PO_4 (85%, 16.49 g) I isobutanol (250 ml) for 16 h. The blue solid was then recovered by filtration and washed with isobutanol. This solid was refluxed for 2 h with distilled water (1 g/9 ml) and the suspension was filtered hot and dried in air (110°C, 16 h) to give a blue solid. VPD was prepared in a two step procedure based on $VOPO_4{\cdot}2H_2O$. $VOPO_4{\cdot}2H_2O$ was prepared by reacting V_2O_5 (5.0 g) with H_3PO_4 (30 ml, 85%) in water (120 ml) under reflux for 24 h. The yellow solid was recovered by filtration, washed sparingly with water, followed by acetone and dried (air, 110°C). $VOPO_4{\cdot}2H_2O$ was then refluxed with predried isobutanol for 20 h (50 mol alcohol/mol $VOPO_4{\cdot}2H_2O$) and the solid product was recovered by filtration and dried (air, 110°C, 16 h).

The oxidation of *n*-butane with the VPA, VPO and VPD catalysts was carried out using a microreactor working under differential conditions using a known volume of catalyst (0.6–0.7 ml). A feedstock composition of butane/oxygen/helium=1.5/18.5/80 and a

total feed gas-flow rate of 1000 ml gas/ml catalyst/h were employed. Reactants and products were analysed by on-line gas chromatography and satisfactory mass balances were obtained for all data presented (98–100%). The following catalyst testing procedure was adopted irrespective of the precursor preparation procedure. The precursor was loaded to the reactor and the flow of the feed gases was established; following this, the precursor was heated to the reaction temperature of 385°C at a rate of 3°C min^{-1}. During this treatment, the catalyst precursor was transformed in situ in the reactor and the catalyst performance gradually improved. The catalyst was allowed to stabilise for 72 h.

2.2. Catalyst characterisation

Catalysts were characterised by powder X-ray diffraction, ^{31}P NMR spin echo mapping and by electron microscopy using scanning and transmission electron microscopy (TEM). The surface areas of the final catalysts were determined using the BET method.

The ^{31}P NMR spin echo mapping spectra were recorded under static conditions, using a $90°$-x-τ-$180°$-y-τ-acquire sequence. The $90°$ pulse was 4.2 μs and τ was 20 μs. For each sample, the irradiation frequency was varied in increments of 100 kHz above and below the resonance of H_3PO_4. The number of spectra recorded was dictated by the frequency beyond which no spectral intensity was observed.

An Hitachi S-2460-N scanning electron microscope was used to obtain topographical information on both the precursors and the final catalysts. Samples, suitable for TEM, were prepared by dispersing the catalyst powder onto a lacey carbon film supported on a copper mesh grid. TEM observations were made in a JEOL 2000EX High Resolution Electron Microscope operating at 200 kV. This instrument was fitted with a low-light-level TV camera and frame averaging system to allow us to use very low illumination conditions. This latter condition is essential for the study of beam sensitive vanadium phosphorus oxide catalysts. Images were recorded on S-VHS videotape, individual frames for which could be, subsequently, captured into a Macintosh Quadra computer for enhancement and detailed analysis.

3. Catalyst structure/activity relationship

One of the most fascinating aspects of oxide catalysts is that there are many different methods by which they can be prepared. For example, WO_3/Al_2O_3 catalysts can be prepared either by incipient wetness impregnation or by adsorption from a tungstate solution [17], MgO can be prepared by burning Mg or by thermal decomposition of the hydroxide, carbonate or basic carbonate [18]. Vanadium phosphate catalysts are no exception and the precursor hemihydrate compound, $VOHPO_4{\cdot}0.5H_2O$, can be prepared by an extensive range of methods [4–9]. Most of the preparations used V_2O_5 and H_3PO_4 as reagents. The initial methods for the preparation of high activity catalysts utilised HCl as a reducing agent using either water or isobutanol as solvents [2,3]. This early research established that the transformation of the hemihydrate precursor to the final catalyst was best carried out in situ in the reactor using the butane/air reaction mixture. The process was recognised as a dehydration and water loss was observed to occur at two temperatures, ca. 360–400 and 460–500°C. It is now known that the transformation of the hemihydrate only involves the higher temperature water loss and the lower temperature process was associated with the decomposition of $VO(H_2PO_4)_2$ which is an impurity present at ca. 10% by mass. Removal of this impurity by water extraction gave improved catalytic performance [19] and this procedure is now standard in many preparations used today. An interesting observation, made for catalysts prepared by using HCl, is that the catalyst performance is mainly a function of surface area and that within experimental error the specific activity of the catalysts is constant even when a range of additives are also included [19].

In our subsequent work, we have studied the morphology of vanadium phosphate catalysts prepared by using three distinctly different methods [11]. The first, denoted by VPA, is the standard aqueous HCl method followed by a water extraction step [10,11]; the second, denoted by VPO, was prepared by the reaction of V_2O_5 with H_3PO_4 in isobutanol followed by a water extraction step [10,11]; the third, denoted by VPD, was prepared by the reaction of $VOPO_4{\cdot}2H_2O$ with isobutanol [10,11]. The three catalysts were then activated in butane air (385°C, GHSV 1000 h^{-1}, 1.5% butane in air) and their catalytic performance

Table 1
Butane conversion to maleic anhydride for VPA, VPO and VPD catalysts [a]

Catalyst	BET area ($m^2\ g^{-1}$)		Conv (%)	Selectivity (%)			Intrinsic activity (10^{-5} mol $m^{-2}\ h^{-1}$)
	precusor	activated		MA	CO	CO_2	
VPA	3	4	11	51	41	7	1.24
VPO	11	14	27	52	34	14	1.35
VPD	32	43	62	64	21	14	1.19

[a] Reaction conditions: 385°C, 1.5% butane/air, 1000 h^{-1}.

and structure were evaluated using a combination of techniques. The catalytic data are shown in Table 1 and the characterisation of the final catalysts using scanning electron microscopy, powder X-ray diffraction and ^{31}P NMR spin echo mapping spectroscopy is shown in Fig. 1, the latter technique is particularly useful in determining the relative proportions of V^{4+}/V^{5+} present. It is clear that the three methods produce very different final structures. A detailed study of the microstructure of the catalysts was carried out by using TEM and high resolution electron microscopy (HREM) and representative micrographs are shown in Fig. 2. Prior to conducting these studies we compiled a standard TEM and HREM atlas of VPO pure phases to enable the identification of the phases present in the catalyst samples. The VPA catalyst was found to contain a complex microstructure in which at least four distinct phases were identified. The majority phase (ca. 80 vol%) was α_{II}-$VOPO_4$ present as 1 μ diameter platelets, and lesser amounts of δ-$VOPO_4$ (10 vol%), $(VO)_2P_2O_7$ (5 vol%) and γ-$VOPO_4$ (5 vol%) were also present. For the VPO catalyst, three distinct morphologies are observed. The major component is oblong $(VO)_2P_2O_7$ crystallites that preferentially expose (100), (021) and (012) faces, together with δ-$VOPO_4$ (20 vol%) and large platelike grains 1–2 μ in diameter of an amorphous 'disorganised' $(VO)_2P_2O_7$. TEM investigation of the VPD final catalyst showed that the material comprised isolated platelets of α_{II}-$VOPO_4$ (3–4 vol%) with the (001) plane preferentially exposed together with the majority of the material being rosette-type agglomerates of $(VO)_2P_2O_7$ (>95 vol%) that preferentially expose the (100) crystal plane. In VPD there was some evidence that a minor fraction of the initial hemihydrate phase (<1 vol%) remained untransformed.

These materials can only be considered to be partially transformed as they have only been activated for 75 h, but it is clear that a range of very different morphologies are displayed by the three preparations. It is, therefore, interesting to observe that the intrinsic activity for the formation of maleic anhydride is almost the same for the three materials (Table 1). In particular, the VPD catalyst comprises a much higher proportion of $(VO)_2P_2O_7$ that preferentially expose the (100) crystal plane (>95 vol%) when compared with the VPO material (<80 vol%), however, the specific activities are almost the same. This leads us to the conclusion that the active sites for the activation of butane and the formation of maleic anhydride can be formed on a broad range of phases.

4. Spectroscopic and electron microscopy studies of the precursor to final catalyst transformation

The transformation of the catalyst precursor to the final catalyst is a crucial aspect of catalyst preparation but there are very few systems for which this has been given much attention. We have studied this transformation in VPO catalysts using two complimentary techniques; namely, in situ laser Raman spectroscopy (LRS) and TEM. The LRS studies were carried out in a specially designed cell [20] in which the vanadium phosphate catalyst is heated in flowing butane/air and the laser Raman spectra were recorded as a function of temperature and activation time. For these studies, we employed the VPA catalyst since no interference from fluorescence was encountered with this material. With VPO type materials, the presence of the organic solvent leads to interference by fluorescence at temperatures below 350°C and the transformation process is less easily followed. At 25°C, the spectrum of $VOHPO_4{\cdot}0.5H_20$ was well defined (Fig. 3) and on heating no significant changes in the spectra were

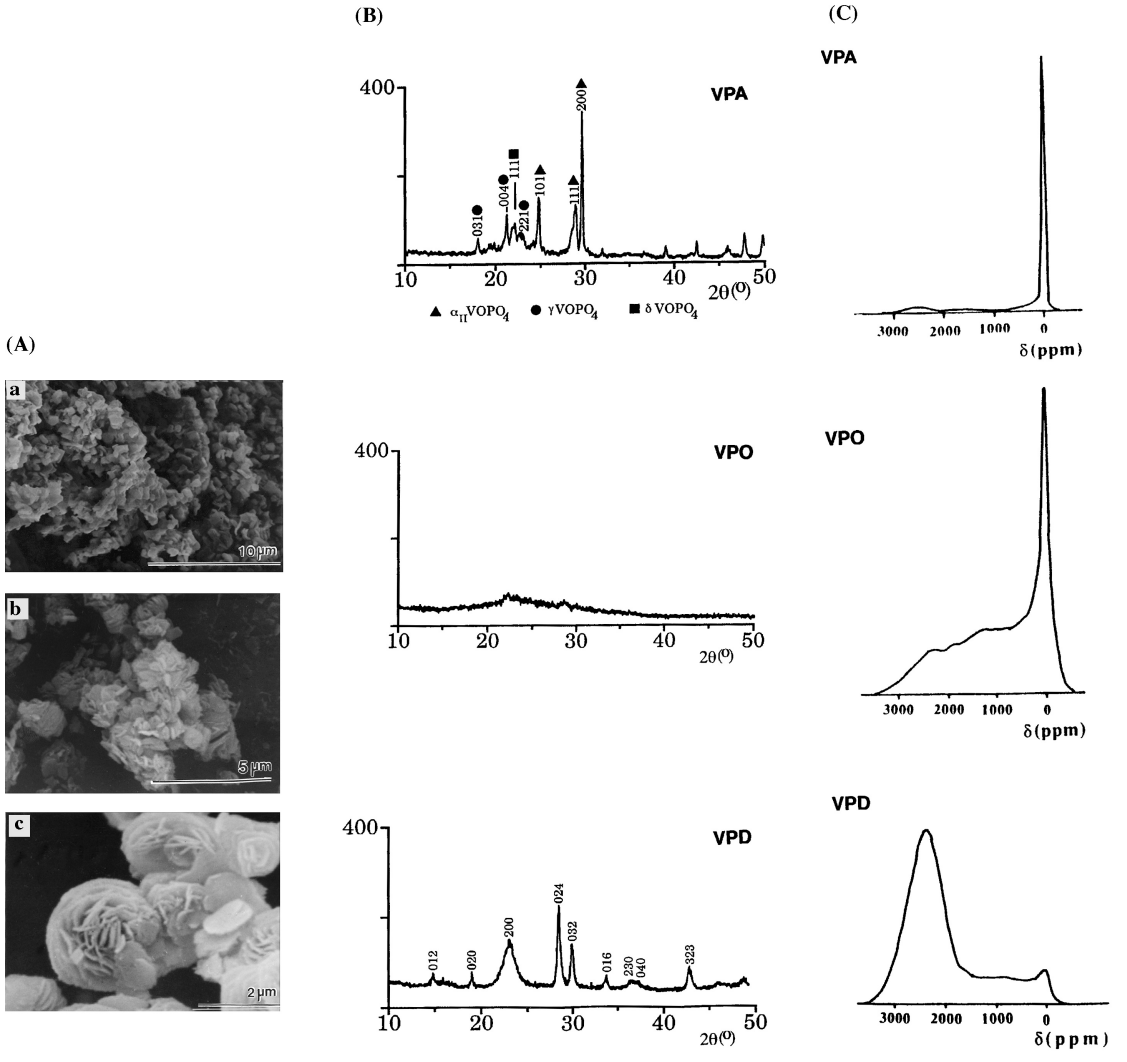

Fig. 1. (a) An SEM micrograph; (b) an XRD pattern; (c) ^{31}P NMR spin echo mapping spectrum from: A, activated VPA; B, activated VPO; and C, activated VPD.

recorded up to 340°C, although the intensity of the Raman scattering decreased and non-selective butane conversion was apparent at 234°C. At 370°C, the material became disorganised and a large number of VPO compounds were observed to be present in this complex structure {$(VO)_2P_2O_7$ α_{II}- and other $VOPO_4$ and non-transformed $VOHPO_4 0{\cdot}5H_2O$}. Subsequent heating at 394°C for 20 h leads to a gradual crystallisation of the catalyst and the catalyst performance improved (Fig. 4) and the final material comprised a mixture of $(VO)_2P_2O_7$, α_{II}-$VOPO_4$ δ-$VOPO_4$ and γ-$VOPO_4$, which is in agreement with the TEM characterisation of this material [11]. The appearance of the V(V) phases was correlated with the onset of maleic anhydride formation and the high degree of disorder is observed only when maleic anhydride is first produced. Detailed studies using the pure VPO compounds observed at this stage of the transformation [21] showed that these materials did not exhibit a loss of Raman scattering due to disorder when examined under identical conditions. This was the first observation that this transformation process was not

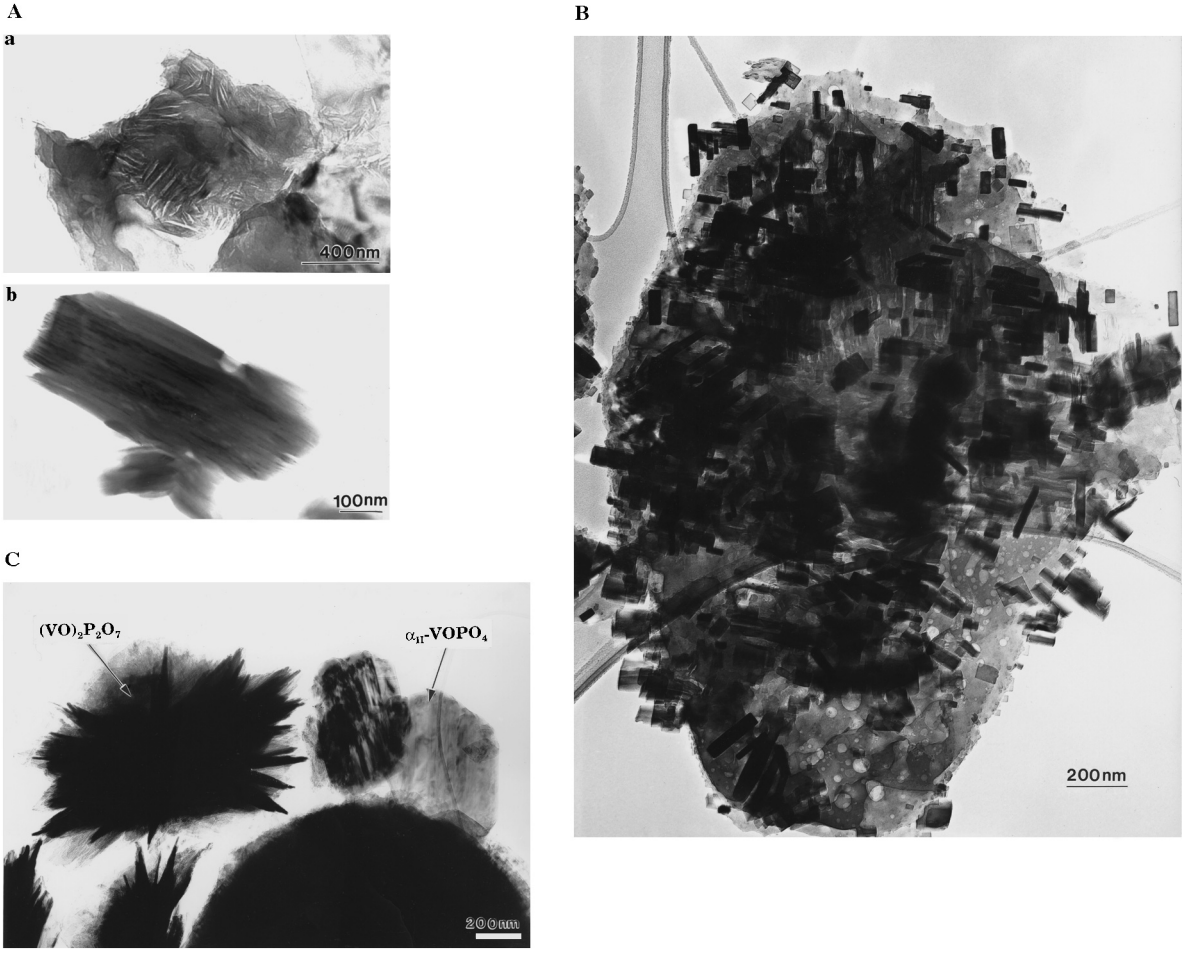

Fig. 2. TEM micrographs of: A, activated VPA; (a) δ-$VOPO_4$, (b) $(VO)_2P_2O_7$; B, activated VPO; and C, activated VPD.

a simple process in which one structure directly transforms into another. Experiments in which maleic anhydride was added to the butane/air pretreatment gases showed that the structural disorder occurred at a lower temperature and, hence, it was concluded [20] that maleic anhydride plays an important role in the establishment of the active catalyst surface.

The hemihydrate to final catalyst transformation has also been characterised in a detailed TEM study [22]. In these experiments, the VPO precursor was selected for investigation, four separate experiments were carried out using the same reaction mixture in a standard laboratory microreactor (n-C_4H_{10}/O_2/He: 1.6/18/80.4) and flow conditions (2.4 l h^{-1} with GSHV=1500 h^{-1}). The temperature was ramped from room temperature to 400°C at a constant rate of 0.5°C min^{-1}. Although the initial treatment was identical for all four experiments, the time-on-stream at 400°C was systematically varied, namely 0.1, 8, 84 and 132 h. The four 'activated' catalysts are denoted by VPO-0.1, VPO-8, VPO-84 and VPO-132, respectively. The catalytic performance data for the four samples activated for different time periods are summarised in Table 2. The n-butane conversion increases from 22 to 65% with increasing activation time. We also observe a decrease in the selectivity for CO and CO_2. It is particularly noticeable that the selectivity to CO decreases very rapidly in the first 10 h. When the variation in surface areas is taken into account, it is apparent that the intrinsic activity for maleic anhy-

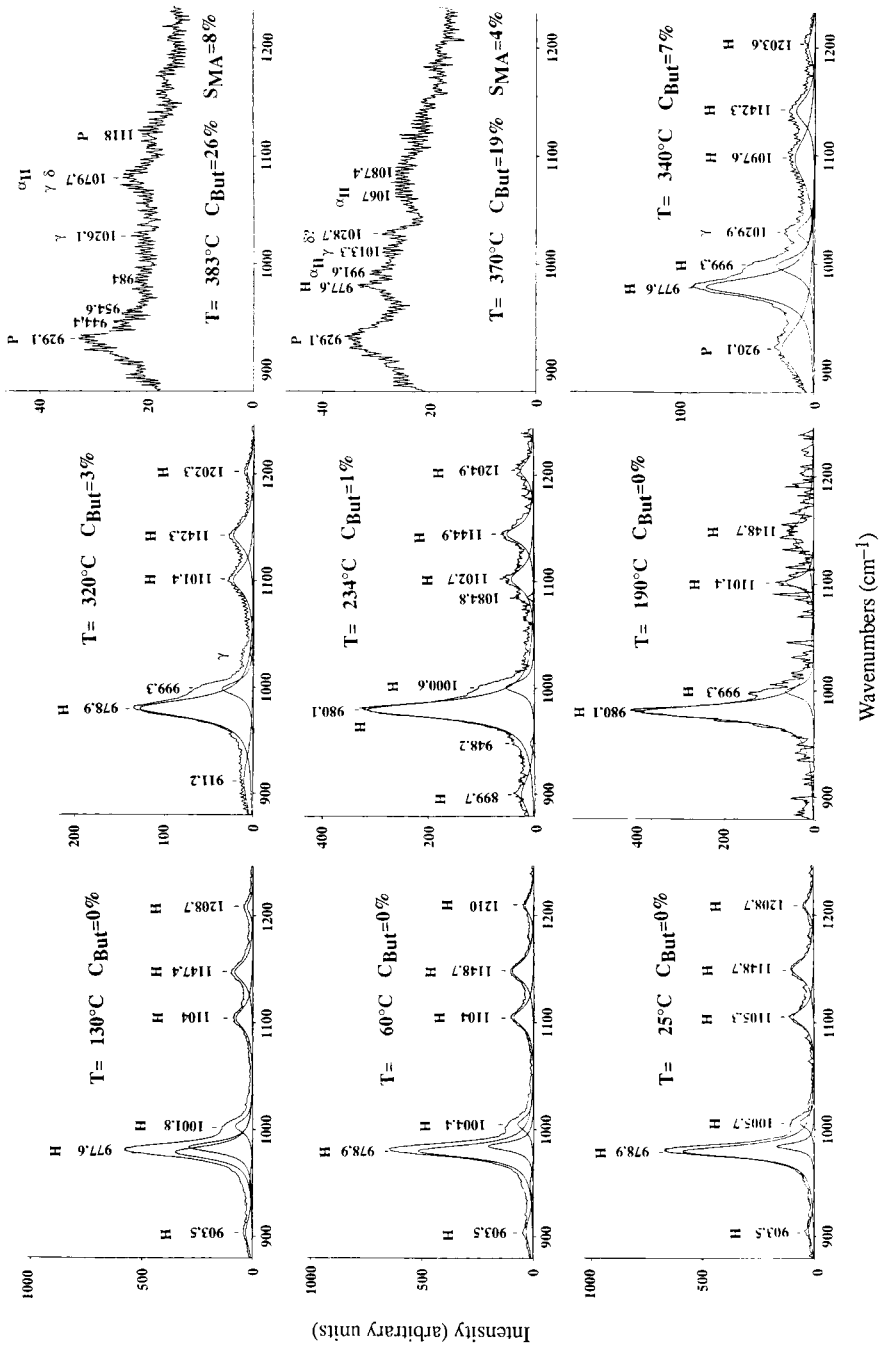

Fig. 3. In situ LRS and catalytic performance data during the activation of VPA in 1.5% butane/air. Key: H, $VOHPO_4{\cdot}0.5H_2O$; P, $(VO)_2P_2O_7$; α_{II}, α_{II}-$VOPO_4$; γ, γ-$VOPO_4$; δ, δ-$VOPO_4$.

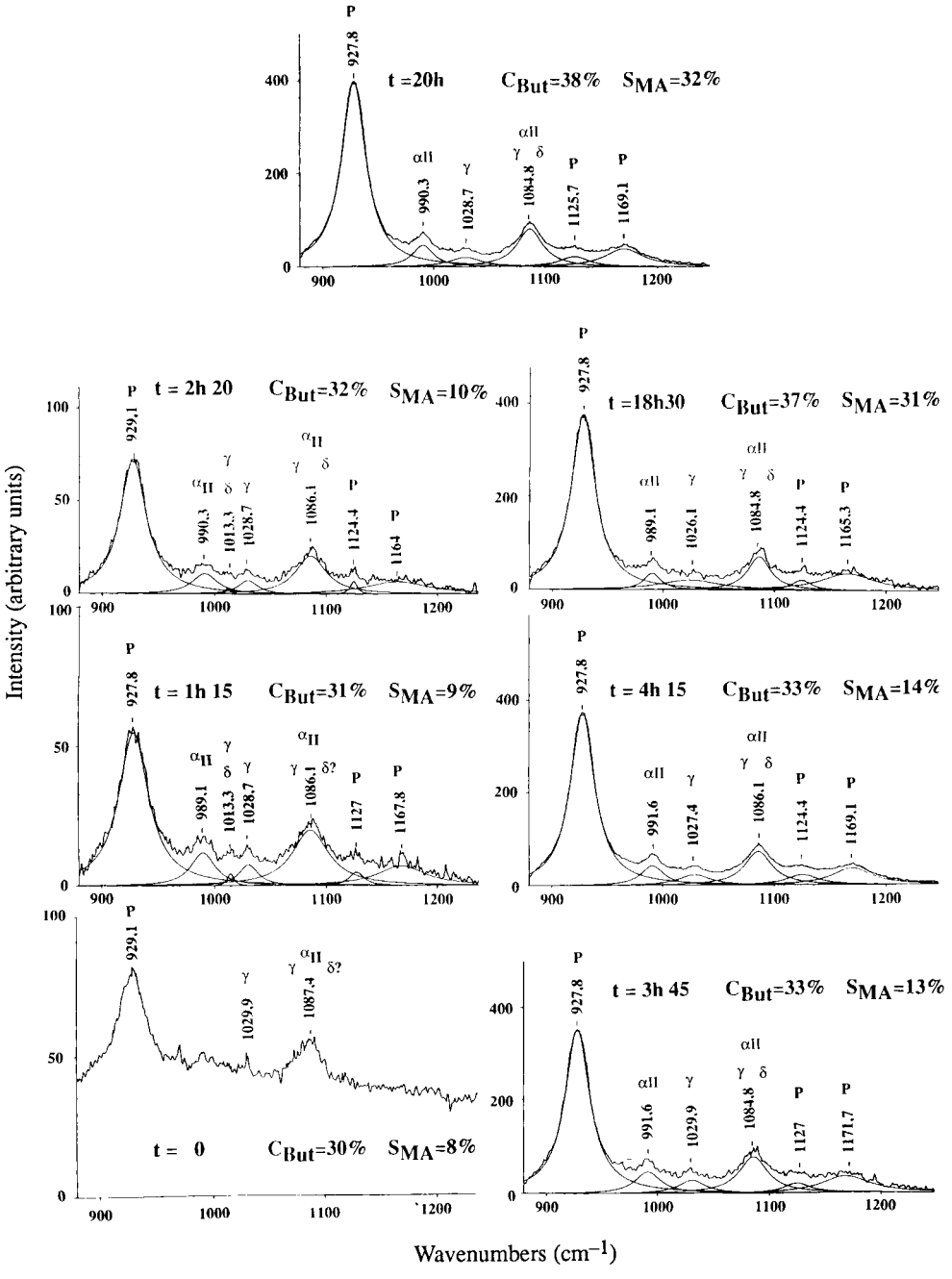

Fig. 4. In situ LRS and catalytic performance data during the activation of VPA in 1.5% butane/air at 394°C. Key as in Fig. 3.

dride production increases steadily with time-on-stream up to 84 h and then tends to level off as the catalyst becomes stabilised. The catalysts were quenched after these different activation times by cooling the reactor rapidly with reactants being present and were then examined using TEM. The VPO precursor comprised rhomboid shaped platelets with thicknesses between 0.03–0.1 μ as shown by TEM

Table 2
Butane conversion to maleic anhydride as a function of increasing activation time

Catalyst	Time-on-stream (h)	BET area ($m^2\ g^{-1}$)	Conv (%)	Selectivity (%)			Intrinsic activity (10^{-8} mol $cm^{-2}\ h^{-1}$)
				MA	CO	CO_2	
VPO-0.1	0.1	10.5	22	34	47	17	0.43
VPO-8	8	7.6	26	48	36	15	0.99
VPO-84	84	14.8	55	66	20	12	1.48
VPO-132	132	19.4	65	69	19	11	1.39

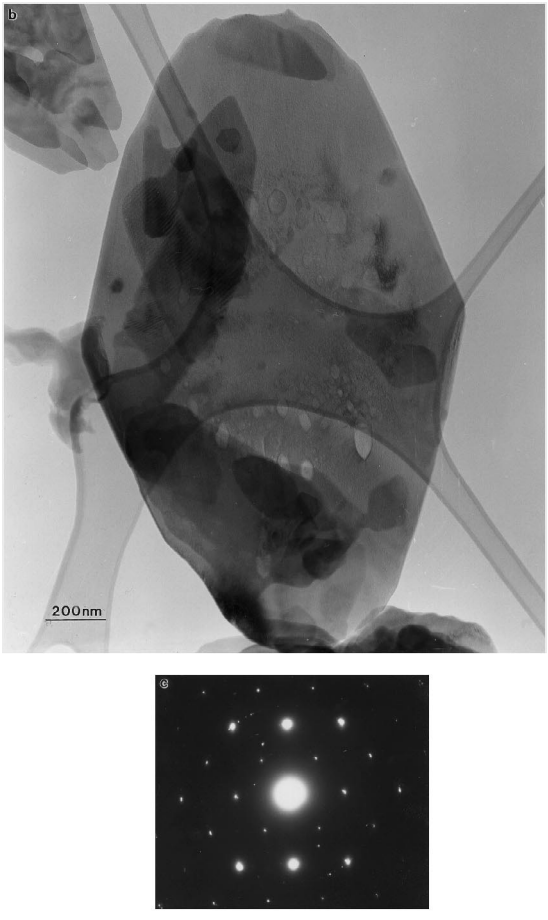

Fig. 5. Bright-field image of the hemihydrate material.

(Fig. 5). Selected area diffraction patterns taken normal to one of these platelets confirmed that the major and minor axes of the rhomboid correspond to the [100] and [010] directions of the $VOHPO_4{\cdot}0.5H_20$ crystal structure, respectively.

Low magnification transmission electron micrographs of typical crystallites from the VPO-0.1, VPO-8, VPO-84 and VPO-132 samples are shown in Fig. 6(a), (b), (c) and (d), respectively. It is clear from the sequence of micrographs that the characteristic rhomboid platelet morphology of the hemihydrate is retained to varying extents in all the specimens. The VPO-0.1 sample (Fig. 6(a)) shows a number of subtle changes from the crystalline hemihydrate platelet. Firstly a number circular features, which are probably internal voids, have appeared. Secondly, isolated patches of the platelet show very characteristic fissures which seem to be crystallographic in origin because they tend to align along the minor axis of the rhomboid platelet. As the activation time increases to 8 h (VPO-8; Fig. 6(b)), the density of circular features markedly increases and a distinct dark fringe ca. 25 nm thick begins to form along the periphery of the platelet. The fringe appears darker than the centre of the platelet due to diffraction contrast, implying that well-crystallised material is nucleating at the platelet rim. The material in the interior of the platelet is much more disordered in character and is very sensitive to electron beam damage. As activation progresses further (VPO-84; Fig. 6(c)), the crystalline fringe at the periphery is now continuous and has coarsened to a thickness of 50–70 nm. Detailed higher magnification studies confirmed that this periphery comprised small crystallites of the pyrophosphate. Furthermore, large holes in the interior of the platelet of up to 300 nm in diameter are now apparent. The residual interior material remains rather disordered and beam sensitive. Finally, the VPO-132 sample in Fig. 6(d) shows the 'end-state' where in addition to the well-crystallised rim, the material in the interior of what remains of the platelet appears more crystalline in character. When the sam-

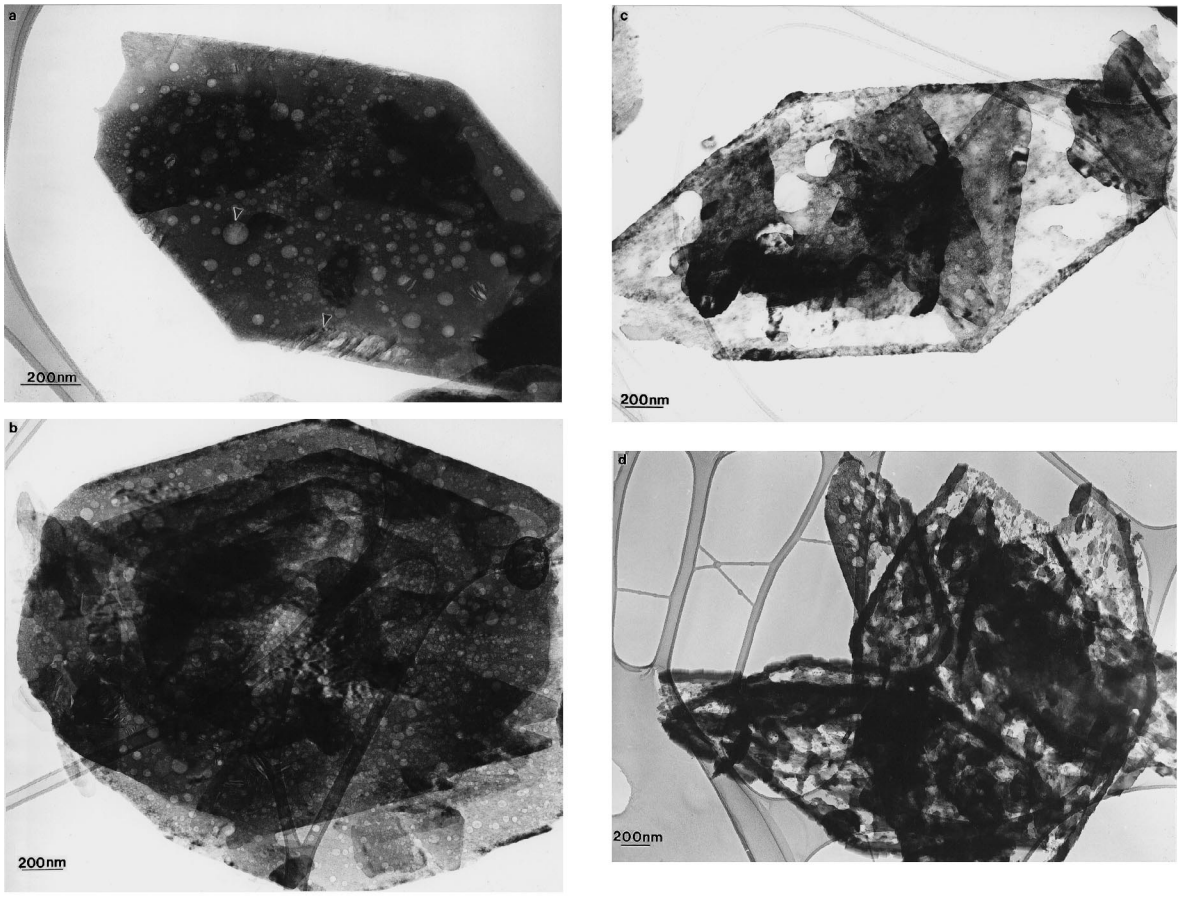

Fig. 6. Bright-field transmission electron micrographs of platelet morphologies in (a) VPO-0.1, (b) VPO-8, (c) VPO-84 and (d) VPO-132 activated catalysts.

ples were analysed at higher magnification (Fig. 7) it is apparent that the rim of the platelet consists small crystallites each ca. 50–100 nm in size. When these are investigated using HREM, analysis of the fringe spacings and intersection angles confirmed that the image (Fig. 7b) was the [100] projection of the $(VO)_2P_2O_7$ phase. Selected area diffraction patterns of the VPO-0.1 sample confirmed the coexistence of $VOHPO_4{\cdot}0.5H_20$, $(VO)_2P_2O_7$ and δ-$VOPO_4$. Furthermore these studies showed that the relative orientations of all three phases are epitaxially related. For instance, the epitaxial orientation relationship between $VOHPO_4{\cdot}0.5H_20$ and $(VO)_2P_2O_7$ is: $[001]^{hemi}//[100]^{pyro}$ and $[010]^{hemi}//[010]^{pyro}$. This orientation relationship has been previously reported in Ref. [22] in terms of the topotactic transformation that can occur between $VOHPO_4{\cdot}0.5H_20$ and $(VO)_2P_2O_7$. However, these studies also indicate that a further topotactic transformation occurs $[001]^{hemi}//[100]^{\delta}$ and $[010]^{hemi}//[001]^{\delta}$.

Since δ-$VOPO_4$ is known to suffer severe beam damage [11], we utilised dark-field imaging of the VPO-0.1 sample in an attempt to locate this phase spatially. The basic principle of the dark-field imaging technique is that a very small objective aperture is inserted into the back focal plane of the microscope which can be used to select only one diffracted beam. This single diffracted beam then passes down the optical axis of the microscope, to form a dark-field image in which only diffracting regions contributing to the selected beam show contrast. Such experiments have the advantage that much lower beam doses are

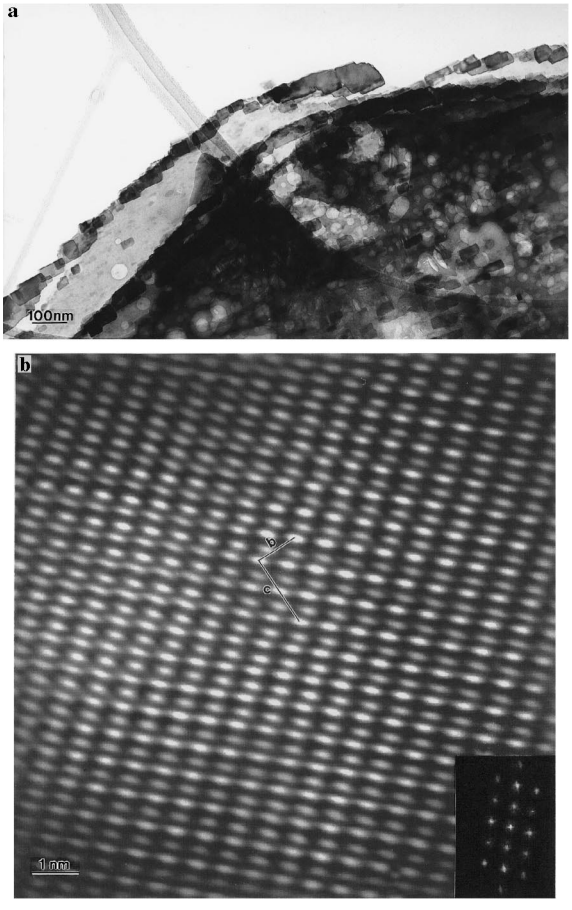

Fig. 7. (a) Bright-field micrograph showing a string of $(VO)_2P_2O_7$ crystallites at the edge of the VPO-84 platelet, (b) an HREM image obtained from one of these crystals which is a characteristic of the [100] projection of $(VO)_2P_2O_7$.

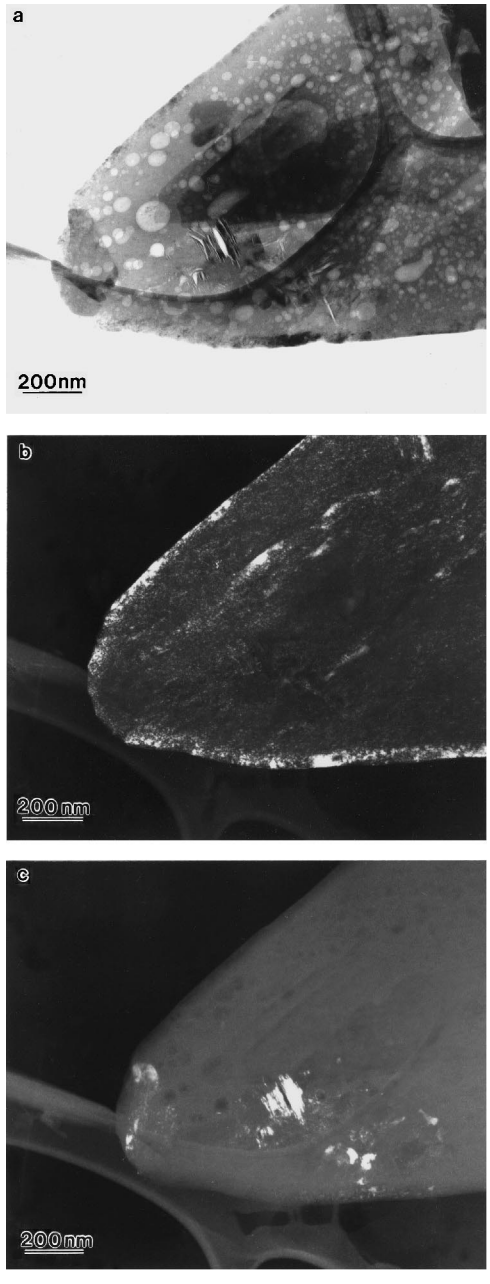

Fig. 8. (a) Bright-field image showing a typical platelet from the VPO-0.1 sample. Corresponding dark field micrographs taken in (b) the g^{pyro} =024 reflection of $(VO)_2P_2O_7$ and (c) the g^{δ}=022 reflection of δ-$VOPO_4$.

employed, but are quite difficult to perform in practise due to the very close proximity of the reflections from different phases in reciprocal space. Fig. 8(a) shows a typical platelet from the VPO-0.1 sample. The corresponding dark-field image shown in Fig. 8(b) was taken in the 024 $(VO)_2P_2O_7$ reflection, in which a thin peripheral fringe of $(VO)_2P_2O_7$ crystallites can be clearly seen. When the 022 δ-$VOPO_4$ reflection is used in this experiment, the occasional crystalline patches, ca. 100–200 nm in diameter, can be seen in the interior of the platelet (Fig. 4(c)). Furthermore, these domains of crystalline δ-$VOPO_4$ phase almost always seem to be associated with the regions of the platelet showing crystallographic fissure features.

In summary, these dark-field imaging experiments suggest that after 0.1 h on stream, crystalline pyrophosphate just begins to form at the rim of the platelet,

whereas the interior seems to consist of very disordered hemihydrate phase in which discrete domains of δ-$VOPO_4$ have nucleated. These domains of δ-$VOPO_4$ and the residual hemihydrate material, subsequently, appear to progressively convert to the pyrophosphate phase with increasing time-on-stream. Simultaneously, the pyrophosphate phase which forms topotactically at the edge of the platelet gradually coarsens and thickens.

Under the particular butane/air transformation conditions we have used, we observe that there are two routes by which the hemihydrate phase can convert to the pyrophosphate phase. At the edge of the platelet a direct topotactic transformation between $VOHPO_4{\cdot}0.5H_20$ and $(VO)_2P_2O_7$ occurs. In the interior of the platelet the transformation between the two phases can occur indirectly via an intermediate δ-$VOPO_4$ phase. As these two types of transformation can apparently occur side by side, it is very likely that small changes in the transformation conditions or the precursor morphology may critically affect the proportion of direct to indirect transformation occurring. To some extent this explains why catalyst samples that have been prepared via different routes and which have not been fully equilibrated show considerably different relative proportions of crystalline $VOPO_4$, crystalline $(VO)_2P_2O_7$ and disordered mixed V^{4+}–V^{5+} phases, as is the case in our VPA, VPO and VPD catalysts.

A further key feature which emerges from our study is that as the time-on-stream increases, the domains of crystalline δ-$VOPO_4$ gradually reduce to the pyrophosphate phase. We have not as yet been able to image this second stage in the transformation to determine whether or not a topotactic change between δ-$VOPO_4$ and $(VO)_2P_2O_7$ occurs. It is interesting to note that ^{31}P NMR MAS and Raman evidence exists [23–26] to suggest that the δ-$VOPO_4$ phase may in some circumstances convert to $(VO)_2P_2O_7$ via an α_{II}-$VOPO_4$ intermediate.

The TEM studies, therefore, confirm the observations made in the in situ LRS studies, i.e. that after a very short exposure to butane/air at >370°C the hemihydrate precursor is transformed into a largely amorphous material which gradually crystallises into $(VO)_2P_2O_7$ and $VOPO_4$ phases. These studies also confirm that the catalyst activity/selectivity are stabilised after a relatively short time (<100 h) when a mixture of V(IV) and V(V) phases are present, although structural changes continue to occur for much longer time periods.

5. Effect of Co^{2+} addition to VPO and VPD catalysts

The catalytic properties of the vanadium phosphorus oxide catalysts can be improved by adding dopants [4,19]. The role of promoters is far from clear since it appears to depend on both their concentration and their mode of introduction into the vanadium phosphorus oxide catalyst. The effect of cobalt has been studied by several groups [4,19,27,28]. It has been observed that this dopant increases the surface area of the catalyst, and it has been suggested that part of cobalt enters the lattice of $(VO)_2P_2O_7$ [4,19,27] which should ensure that the active catalyst contains the excess phosphorus required to maintain its stability in an oxidising environment. XPS measurements have revealed that the surface of the catalysts is enriched with phosphorus [28]. Another proposal for the role of cobalt, at low concentration, is that an average oxidation state of vanadium could be maintained by a redox effect and this would enable improved initial dehydrogenation of *n*-butane, and control of oxygen diffusion thereby minimising the non-selective oxidation route [4].

We studied the effect of adding cobalt at low concentration (5% Co/V) on the catalytic and physicochemical properties of the two series previously denoted by VPO and VPD [13,29]. Cobalt was introduced as the acetylacetonate salt, dissolved into isobutanol, during the preparation of the precursors in order to favour the dispersion of the dopant into the bulk structure. The in situ LRS study of the activation under *n*-butane air of the Co-doped VPO precursor revealed that maleic anhydride appeared in the gas effluents at lower temperature (235°C) as compared to the undoped catalyst (400°C). This was associated with the detection of the Raman signal at 1091 cm^{-1} characteristic of $VOPO_4$ structures (α_{II}, γ and δ) while the signal of $(VO)_2P_2O_7$ at 1176 cm^{-1} was not detected at this low temperature [29]. It was observed that maleic anhydride could be produced in the presence of V^{5+} sites while the $VOHPO_4{\cdot}0.5H_20$ precursor (signal at 984 cm^{-1}) was not yet fully

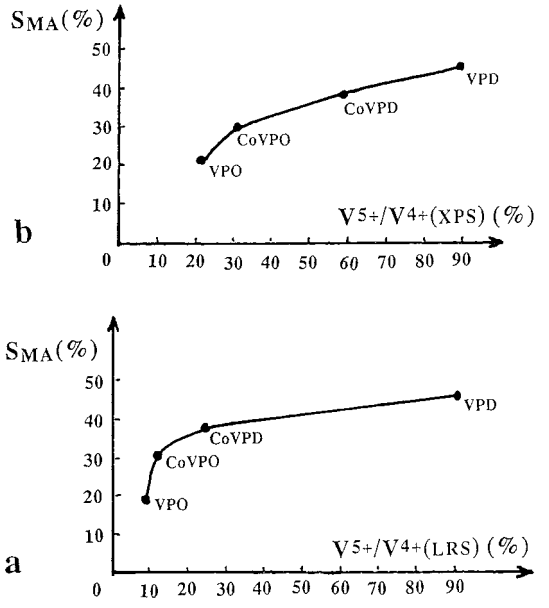

Fig. 9. Selectivity to maleic anhydride (S_{MA}) vs. (a) V^{5+}/V^{4+} ratio (from LRS) and, (b) V^{5+}/V^{4+} ratio (from XPS).

decomposed. For the VPD and the Co-doped VPD precursor, maleic anhydride was observed as soon as Raman signals at 1038 cm^{-1} (α_I-$VOPO_4$) and 1094 cm^{-1}(α_{II}, γ and δ-$VOPO_4$) were detected [13]. The V^{5+}/V^{4+} ratio could be evaluated from the LRS study by the relative ratio of the intensity of the characteristic bands associated with $VOPO_4$ (1034 cm^{-1} for α_I-VOPO4 and 1091 cm^{-1} for α_{II}-VOPO4) and with $(VO)_2P_2O_7$ (1176 cm^{-1}). The selectivity to maleic anhydride is plotted (Fig. 9a) for four VPO, CoVPO (Co/V =5%), VPD, CoVPD (Co/V =5%) catalysts after 78 h time-on-stream with a butane/air atmosphere vs. the V^{5+}/V^{4+} as measured by LRS. These catalysts gave comparable level of butane conversion (ca. 30%). A monotonic correlation is observed between the selectivity for maleic anhydride (S_{MA}) and the V^{5+}/V^{4+} ratio. The same type of correlation, with the same order for the catalysts is observed when plotting S_{MA} vs. the V^{5+}/V^{4+} ratio (Fig. 9b) as determined from the $V_{2p3/2}$ contributions of the V^{5+} and V^{4+} XPS signals observed at 518.0 and 516.9 eV, respectively. These two in situ Raman studies and the XPS measurements provide clear evidence for the important role of V^{5+} sites in the production of maleic anhydride.

6. Comments on the nature of the active site

The key results from our studies can be summarised as follows:

(a) The observation of similar specific activity for the VPA, VPO and VPD catalysts indicates that the active site can be formed on a wide range of vanadium phosphorus containing phases.
(b) The detailed in situ LRS and TEM studies show that the hemihydrate to final catalyst transformation is complex and that after a short exposure to butane air at temperatures >370°C the hemihydrate is transformed to a mainly disordered material. At the onset of maleic anhydride formation there is a complex mixture of phases present including $(VO)_2P_2O_7$ and $VOPO_4$ phases.
(c) The detailed studies with Co^{2+} promoted VPO and VPD catalysts show that the activity for maleic anhydride formation is a function of the concentration of the V(V) phases present.

From these studies we conclude that the active centre for butane activation and maleic anhydride formation comprise a V^{4+}/V^{5+} couple that is well dispersed on the surface of a range of VPO phases, which for well-equilibrated catalysts will be $(VO)_2P_2O_7$. It is possible that the active site could be at a defect site as indicated in the studies of Gai and Kourtakis [30] or alternatively it is possible that a contact synergy between well-dispersed microcrystalline $VOPO_4$ phases (i.e. non detectable by XRD) and well-crystalline $(VO)_2P_2O_7$ may also play a role. Recent studies have also confirmed the importance of V(V) phases. Coulston et al. [16] have used time resolved in situ X-ray absorption spectroscopy and have shown that when either α_I-$VOPO_4/SiO_2$ or $(VO)_2P_2O_7/SiO_2$ catalysts are exposed to butane, the rate of maleic anhydride formation is directly correlated with the decay in the concentration of the V^{5+} species in the catalyst. This supports the hypothesis that V(V) is important for the selective activation of butane to maleic anhydride. However, the exact nature of the active sites (dispersed V^{5+} or small $VOPO_4$ domains with a limited size and crystallinity on the $(VO)_2P_2O_7$ matrix) is still a matter of debate.

Acknowledgements

We thank the EC HCM programme (Contract CHRX-CT92-0065) EPSRC and the industrial affiliates of the Leverhulme Centre for financial support. We also thank Su Sajip, Michel Abon, Alain Tuel and Kossi Béré for experimental studies and discussions.

References

[1] R.L. Bergman, N.W. Frisch, US Patent 3293268 (1966), assigned to Princeton Chemical Research.
[2] J.P. Harrison, US Patent 3985775 (1976), assigned to Chevron Research Co..
[3] R.A. Schneider, US Patent 3864280 (1975), 4043943 (1977) assigned to Chevron Chemical Research.
[4] G.J. Hutchings, Appl. Catal. 72 (1991) 1.
[5] J.W. Johnson, D.C. Johnson, A.J. Johnson, J.F. Brady, J. Am. Chem. Soc. 106 (1984) 8123.
[6] H. S Horowitz, C.M. Blackstone, A.W. Sleight, G. Truffer, Appl. Catal. 38 (1988) 193.
[7] E. Bordes, Catal. Today 3 (1988) 163.
[8] I.J. Ellison, G.J. Hutchings, M.T. Sananés, J.C. Volta, J. Chem. Soc., Chem. Commun. (1994) 1093; M.T. Sananés, G.J. Hutchings, J.C. Volta, J. Chem. Soc., Chem. Commun. (1995) 243.
[9] G.J. Hutchings, M.T. Sananés, S. Sajip, C.J. Kiely, A. Burrows, I.J. Ellison, J.C. Volta, Catal. Today 33 (1997) 161.
[10] G.J. Hutchings, R. Olier, M.T. Sananés, J.C. Volta, Stud. Surf. Sci. Catal. 82 (1994) 213.
[11] C.J. Kiely, A. Burrows, S. Sajip, G.J. Hutchings, M.T. Sananés, A. Tuel, J.C. Volta, J. Catal. 162 (1996) 31.
[12] G.J. Hutchings, I.J. Ellison, J. Bartley, M.T. Sananés, S. Sajip, C.J. Kiely, A. Burrows, J.C. Volta, Catal. Today, 40.
[13] M.T. Sananés, F. Ben Abdelouahab, G.J. Hutchings, J.C. Volta, J. Catal. 163 (1996) 346.
[14] W.V. Guliants, J.B. Benziger, S. Sundaresan, I.E. Wachs, J.-M. Jehng, J.E. Roberts, Catal. Today 28 (1996) 275.
[15] I.E. Wachs, J.-M. Jehng, F. Deo, B.M. Weckhuysen, W.V. Guliants, J.B. Benziger, Catal. Today 32 (1996) 47.
[16] G.W. Coulston, S.R. Bare, H. Kung, K. Birkeland, G.K. Bethke, R. Harlow, N. Herron, P.L. Lee, Science 275 (1997) 191.
[17] A.M. Maitra, N.W. Cant, D.L. Trimm, Appl. Catal. 27 (1966) 9.
[18] J.S.J. Hargreaves, G.J. Hutchings, R.W. Joyner, C.J. Kiely, J. Catal. 135 (1992) 576.
[19] G.J. Hutchings, R. Higgins, J. Catal. 162 (1996) 153.
[20] G.J. Hutchings, A. Desmartin-Chomel, R. Olier, J.C. Volta, Nature (London) 368 (1994) 41.
[21] F. Ben Abdelouahab, R. Olier, N. Guilhaume, F. Lefebvre, J.C. Volta, J. Catal. 134 (1992) 151.
[22] C.J. Kiely, A. Burrows, G.J. Hutchings, K.E. Béré, J.C. Volta, A. Tuel, M. Abon, J. Chem. Soc., Faraday Disc., in press.
[23] J. Li, M.E. Lashier, G.L. Schrader, B.C. Gerstein, Appl. Catal. 38 (1988) 83.
[24] M. Abon, K.E. Béré, A. Tuel, P. Delichere, J. Catal. 156 (1995) 28.
[25] M.T. Sananés, A. Tuel, J.C. Volta, J. Catal. 145 (1994) 251.
[26] J.C. Volta, K. Biri, Y.J. Zhang, R. Olier, ACS Symposium Series, Vol 523, p. 217 (S.T. Oyama, J.W. Hightower, Eds.), Am. Chem. Soc., Washington, DC, 1993.
[27] B.K. Hodnett, B. Delmon, Appl. Catal. 6 (1983) 245.
[28] V.A. Zazhigalov, J. Haber, J. Stoch, A.I. Pyatnitzkaya, G.A. Komashko, V.M. Belousov, Appl. Catal. 96 (1993) 135.
[29] F. Ben Abdelouahab, R. Olier, M. Ziyad, J.C. Volta, J. Catal. 157 (1995) 687.
[30] P.L. Gai, K. Kourtakis, Science 267 (1995) 661.